Journal of Energy and Power Engineering 13 (2019) 249-266
doi: 10.17265/1934-8975/2019.07.001

Study of Effective Electrical Conductivity of Additive Free Electrodes Using a Homogenization Method

Subash Dhakal[1] and Seshasai Srinivasan[1,2]

1. Department of Mechanical Engineering, McMaster University, Hamilton, ON L8S 4L8, Canada

2. School of Engineering Practice and Technology, McMaster University, Hamilton, ON L8S 4L8, Canada

Abstract: Conductive additives are used in the cathode of a Li-ion battery to improve electrical conductivity. However, these additives can negatively impact the ionic conductivity and specific capacity of the battery. Therefore, design of additive-free cathodes is gaining attention in the research community. In this paper, we explore the effective electrical conductivity of randomly generated two-phase conductive-free cathode microstructures using a mathematical homogenization method. Over thousand microstructures with various combinations of particle size, volume fraction and conductivity ratios are considered to evaluate effective electrical conductivity values using this method. An explicit formulation is proposed based on the results to provide a simple method for evaluation of the effective conductivity values. The intrinsic properties of each phase of the microstructure are used to obtain the effective electrical conductivity values. With the microstructure geometry information being utilized for the evaluation of the effective properties, the results obtained from this formulation are expected to be more accurate and reliable than those obtained using the popular Bruggeman's approximation, providing better estimates of discharge characteristics. Finally, the significance of incorporation of micro-structural information to model cathodes is highlighted by studying the discharge characteristics of Li-ion battery system.

Key words: Lithium ion, additive-free electrode, homogenization, effective conductivity, Bruggeman, particle size.

List of Symbols

σ^*	Effective conductivity, S/m
σ	Intrinsic conductivity, S/m
ε	Volume fraction of conductive phase
ε_j	Volume fraction of "j" phase
γ	Bruggeman's exponent
τ	Tortuosity
r	Domain length normalized particle size
$r_{p/n}$	Actual particle size, μm
N	Number of particles
h	Conductivity ratio
L	Length of domain

Subscripts

AP	Active particles
E	Electrolyte
p	Positive electrode
n	Negative electrode

Corresponding author: Seshasai Srinivasan, PhD, Chair, research fields: software engineering technology, CFD, heat transfer, lithium batteries.

1. Introduction

With a rapidly increasing population, which is estimated to be around 7.5 billion by the end of 2017, the demand for energy is ever increasing. It is estimated that the energy demand for the world will increase by 48% in 2040 as compared to the demand in 2012 [1]. However, based on the World Energy Council (WEC) report, only about 14% of the world's energy demand was met by renewable energy sources including hydropower in 2015 [2]. Currently, due to our over-reliance on the traditional energy sources like coal and gas to meet this demand, atmospheric carbon dioxide levels are at an all-time high resulting in global warming and climate change. Hence, current focus in the research community is in the development of clean and renewable energy resources in order to overcome this problem. Renewable energy systems, including solar and wind energy, and electric vehicles require efficient and high-capacity energy storage systems. Lithium-ion (Li-ion) batteries are the batteries of

choice in these applications as well as in consumer electronics such as laptops, cell phones, etc. because they offer a lot of advantages over other rechargeable battery systems. Li-ion batteries have very high specific energy storage capacity, negligible memory effects and lower self-discharge rate as compared to other rechargeable battery systems [3].

In order to improve the features such as storage capacity and rate of discharge of Li-ion batteries, extensive research has taken place with a focus to improve the properties of electrodes. Research in this field involves the improvement of materials used in electrolytes and electrodes to make them more cost-competitive and efficient. Typically, a Li-ion battery consists of the positive and negative electrodes, electrolyte and a separator. During the charge cycle, Li-ion is inserted into the negative electrode during charge and extracted from it during the discharge cycle. Transfer of Li-ions across the electrodes takes place simultaneously with the transfer of electrons from the outer circuit. There are several types of Li-ion batteries in use in the market currently. The intended application determines the chemistry, performance and cost characteristics. Typically, the positive electrode consists of a Lithium metal oxide ($LiFePO_4$, $LiMn_2O_4$, etc.) and the negative electrode is made up of graphite. The separator holds these two electrodes apart and is made up of a permeable membrane. It allows the Li-ion to pass through it but blocks the flow of electrons hence avoiding short-circuiting. The electrolyte comprises of lithium salts ($LiPF_6$, $LiBF_4$, etc.) in an organic solvent that is typically composed of ethylene carbonate and dimethyl carbonate (EC: DMC). Positive electrode is porous with electrolytes residing in pores and is made up of active particles which are held together by binder [4, 5].

Additionally, carbon particles are added along with the binders to increase the overall electronic conductivity of the cathode of Li-ion batteries. Although these carbon additives help enhance the electrical conductivity, they can have a negative effect on the ionic conductivity. These additives can occupy anywhere between 10%-40% of the weight of the entire electrode [6]. However, since these additives are not directly involved in the electrochemical reactions, they limit the specific energy capacity of the cell. These additives create difficulty in modeling of the transport of Li-ions and electrons. Therefore, it is desirable to design Li-ion battery cathodes without the inclusion of these conductive additives. Ha et al. [6] provided a process for the fabrication of additive-free high performance cathodes using nanoparticles.

An alternative approach to improve the performance of a battery without using additives would be to develop optimally engineered microstructures. It is well known that one of the key factors affecting the electrical conductivity is the size and distribution of active particles. Liu et al. [7] found that the reduction in the size of active particles significantly increases the rate capability of Li-ion batteries. Use of nanomaterials for battery electrodes can significantly boost the electrochemical properties of the battery by enhancing the reversible Li-ion intercalation process. This leads to the enhancement of the reversible Li-ion intercalation process [7]. Consequently, smaller particle sizes are desired for cathode microstructures. However, because of the concern over safety and stability due to larger surface area of the nano-sized particles, control of the size of active particles is considered to be an important part in the design of cathode microstructure [8]. Another important factor to be considered for the design of the cathode microstructures is the particle polydispersity [9]. Taleghani et al. [10] found that the cell capacity, voltage and specific power of a battery are significantly affected by the multi-modal particle size distribution. Similarly, Garcia et al. [11] found that higher power densities can be obtained by using a homogeneous, small and well-dispersed active particle size distribution.

Simulation of electrochemical and thermal properties provides a cost-effective and time-saving avenue for the design of optimal battery systems. This process

is employed using robust and efficient mathematical models and is based on the laws of physics and chemistry. There are several methods that can be used to carry out the simulation of Li-ion batteries. Use of a certain method depends on the desired application and is determined by the computational cost and desired accuracy. Single-particle model, pseudo-two-dimensional model (P2D), multi-physics and molecular/atomistic models most widely used electrochemical models extensively referred to in literature [12]. The constituents of the battery are high-range multi-scale in nature. As a result, it is computationally infeasible to carry out a detailed direct simulation utilizing the properties of all the elements that constitute a Li-ion battery [13]. Hence, batteries are modeled using effective transport properties of electrodes with the incorporation of the information of transport properties of all the constituent phases.

The most extensively used method to evaluate the transport properties is based on the effective medium theory proposed by Bruggeman [14]. The transport property of interest in this paper is the effective electrical conductivity, which, based on the Bruggeman's formula can be written as [13, 15, 16]:

$$\sigma^* = \sigma\varepsilon^{\gamma} \quad (1)$$

where Bruggeman's exponent, $\gamma = 1.5$. Similarly, σ^* is the effective conductivity and σ and ε are the actual conductivity and volume fraction of the conductive material. However, this formula fails to incorporate the effects of the microstructure geometry arrangement on the effective values [17]. The microstructure of the electrode of a Li-ion battery can undergo major changes during a typical operating cycle. This, in turn, can strongly affect the effective properties even when the volume fraction essentially remains the same. Therefore, evaluation of effective properties of the microstructure of a typical Li-ion battery electrode, which has a complicated geometry, based on this method is unreliable. Knowing this, the value of γ is often adjusted to better predict the effective properties including conductivity and diffusivity of porous electrodes. For example, Doyle et al. [18] used higher values of γ to better estimate the effective transport properties. Vadakkepatt et al. [16] obtained different values of the Bruggeman's exponents for evaluation of effective thermal conductivity by using numerical simulation of fully resolved cathode microstructures of Li-ion battery.

In this paper, we use a mathematical homogenization method, inspired by the work by Gully et al. [13], to evaluate the effective electrical conductivity of random microstructures with two phases. In this method, the microstructure information along with the individual phase properties is used to calculate the effective transport properties of the complex composite microstructures. We focus our study on the evaluation of effective electrical conductivity of Li-ion battery electrodes considering only two phases namely the conducting active phase and the non-conducting electrolyte phase to mimic additive-free cathodes.

The rest of the paper is organized as follows. In Section 2, we describe the theory behind the homogenization-based formulation. Detailed description of the method used in the generation of the microstructure is given in Section 3. In the Evaluation of Effective Conductivity section, we provide the results of the simulation used to evaluate the effective electrical conductivity values of the generated microstructures. We also show comparison of the results with Weiner bounds and Bruggeman's theory. Based on the results of the previous sections, we proceed to propose an algebraic formulation for the evaluation of the effective electrical conductivity of two-phase microstructures in the next section. In the Analysis of Proposed Formulation section, we provide detailed error analysis of the proposed formulation. In the subsequent section, we illustrate the application of the algebraic formulation by studying the discharge characteristics of an idealized Li-ion battery model. Finally, we summarize the findings of this paper and end with a note on future work.

2. Mathematical Homogenization Formulation of the Effective Transport Properties

For mathematical homogenization, the following assumptions are made on the microstructure domain Ω_0:

(a) Ω_0 is periodic in all three directions.

(b) Ω_0 is a union of three sub-domains Ω_1, Ω_2 and Ω_3 which represent the three distinct phases, i.e., $\Omega_0 = \Omega_1 U \Omega_2 U \Omega_3$.

(c) Each of the phases Ω_j, $j = 1, 2, 3$, is isotropic.

(d) The individual phases are characterized by non-zero conductivity coefficients σ_j ($j = 1, 2, 3$), such that:

$$\sigma(\mathbf{x}) = \sigma_1\chi_1(\mathbf{x}) + \sigma_2\chi_2(\mathbf{x}) + \sigma_3\chi_3(\mathbf{x}) \tag{2}$$

$$\chi_j(\mathbf{x}) := \begin{cases} 1\ \mathbf{x} \in \Omega_j, \\ 0\ \mathbf{x} \notin \Omega_j \end{cases} \tag{3}$$

where χ_j is the characteristic function of the j-th phase (“: =” means “equal by definition”).

The Ohm’s law can be written as

$$\mathbf{J}(\mathbf{x}) = \sigma(\mathrm{x})\mathbf{E}(\mathbf{x}) \tag{4}$$

where **J** and **E** represent the current and electric fields respectively while σ(x) is defined in Eq. (3). Since there are no sources or sinks of charge within the material and electric field is simply the negative gradient of the electric potential, we can write:

$$\nabla \times \mathbf{E}(\mathbf{x}) = \mathbf{0} \text{ and } \nabla.\mathbf{J}(\mathbf{x}) = 0. \tag{5}$$

Let

$$\langle \mathbf{E} \rangle = \mathbf{e}_k, \tag{6}$$

where $_k$ is a unit vector in the k-th direction for $k = 1, 2, 3$. We can re-write Ohm’s law as:

$$\langle \mathbf{J} \rangle = \sigma^* \langle \mathbf{E} \rangle \tag{7}$$

Here, $\langle \cdot \rangle$ is the spatial average over a periodic microstructure Ω_0. Following the mathematical transformations described by Gully et al. [13], we can write the electric field **E** as:

$$\mathbf{E} = \left[\mathbf{I} + s_1^{-1}\boldsymbol{\Gamma}\chi_1 + s_2^{-1}\boldsymbol{\Gamma}\chi_2\right]^{-1}\mathbf{e}_k, \tag{8}$$

where

$$s_1^{-1} := 1 - \sigma_1/\sigma_3 \text{ and } s_2^{-1} := 1 - \sigma_2/\sigma_3 \tag{9}$$

Here **I** represents the identity operator. Also for arbitrary vector field **z**, the operator $\boldsymbol{\Gamma}$ is defined as:

$$\boldsymbol{\Gamma}\mathbf{z} := \nabla(-\Delta)^{-1}\nabla.\mathbf{z} \tag{10}$$

On denoting $\sigma^* = [\sigma^*]_{kk}$ as the kk-th component of the effective conductivity tensor, it can be shown that:

$$[\sigma^*]_{kk} = \sigma_3\left[1 - \langle e_k^T\left(s_1^{-1}\chi_1 + s_2^{-1}\chi_2\right)\left[\mathbf{I} + s_1^{-1}\boldsymbol{\Gamma}\chi_1 + s_2^{-1}\boldsymbol{\Gamma}\chi_2\right]^{-1}\mathbf{e}_k\rangle\right] \tag{11}$$

Numerical solution of Eq. (11) subject to periodic boundary conditions provides the desired effective conductivity tensor for any geometric configuration. Microstructure geometry information is imported as functions χ_1, χ_2 and χ_3. Thus, unlike the Bruggeman’s formula, this approach clearly utilizes the geometric information of all the phases including the information of individual conductivities. Although we have discussed the formulation for three distinct phases, this approach can be easily implemented to study two-phase microstructure geometry. All our effective conductivity value calculations utilize the numerically implemented form of Eq. (11) for two-phase cases. The information of microstructure is extracted from the 2D images generated as explained in the following section.

3. Representative Microstructure Generation

In this section, we describe the methodology employed for the generation of the two-phase microstructures used in this study. As shown schematically in Fig. 1a, the positive electrode of a Li-ion battery consists of three phases namely active particles (Ω_{AP}), binder (Ω_B) and electrolyte (Ω_E). However, for this two-phase study, we only consider the active particles and electrolyte phase which resides in the electrode pores to represent the conductive additive-free cathodes. This is also in line with the aim of the paper to provide a qualitative insight into the effects of microstructure geometry in the effective electrical conductivity of the electrode. The two phases are denoted as solid

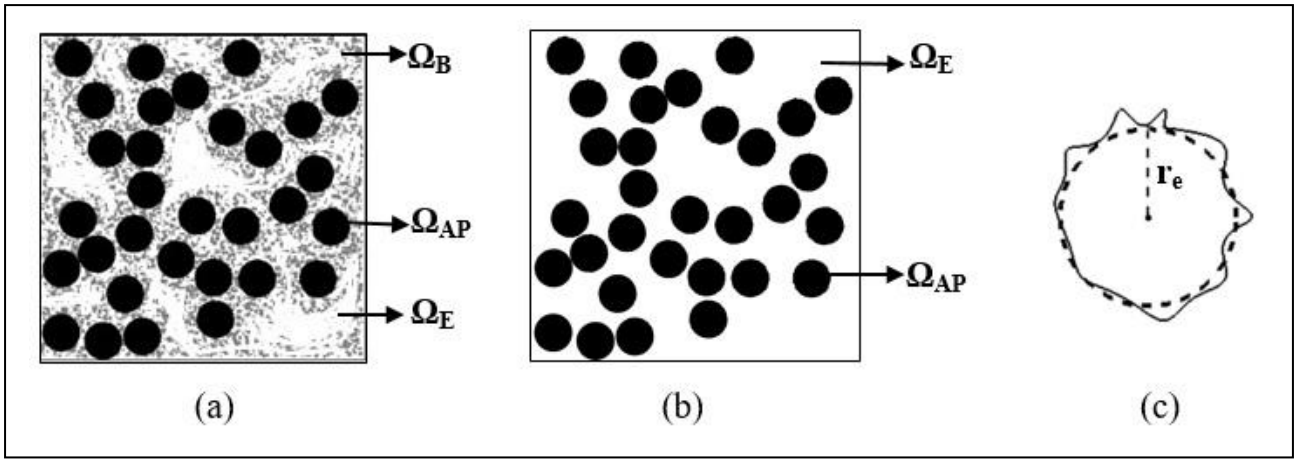

Fig. 1 (a) A micro-scale schematic diagram showing components of Li-ion cell positive electrode consisting of active particles (ΩAP), binder (ΩB) and electrolyte (ΩE) represented by black, gray and white colors respectively. (b) Schematic of microstructure used for study with black shapes representing active particles (ΩAP) and white space representing electrolyte (ΩE). (c) Representation of effective radius (re) of an arbitrary solid phase particle.

phase (Ω_{AP}) which represents the active particles and electrolyte phase (Ω_E) as shown in Fig. 1b.

We now introduce a key parameter called particle size which is used to define the microstructure size for different particle shapes used in this paper. The particle size r is defined as the distance from the center of a solid phase particle to its circumference and is a domain-normalized parameter. For circular particles, this is simply the radius divided by the domain length. In general, this parameter is given by the equivalent radius (r_e) which is defined as the radius of a circle of same area of the actual particle given by $A_{\Omega_{AP}}$ as shown in Eq. (12). As described earlier, the value of r is domain length normalized. For example, for the electrode of width 5 μm, $r = 0.05$ represents the actual particle size of $r = 0.01$ μm. Similarly, conductivity ratio is defined as the ratio of the actual conductivity values of the solid phase and electrolyte phase as given in Eq. (13). The volume fraction ε_{AP} is simply the fraction of area occupied by the solid phase active particles in any given microstructure.

$$r = r_e = (A_{\Omega_{AP}}/\pi)^{1/2} \quad (12)$$

$$h = \sigma_{AP}/\sigma_E \quad (13)$$

To provide a complete picture of the effects of volume fraction and particle size on effective conductivity, random microstructures were generated across a range of volume fractions and particle sizes in MATLAB [19]. Sample microstructures are shown in Fig. S1. The complete range of values covering a wide spectrum of r, h and ε_{AP} used in the study is presented in Fig. S2 of the supplementary material. Randomly generated circular particles with irregular edges are used to represent the solid-phase of an electrode. To account for the potential variety in a microstructure with a given volume fraction, three different microstructural images with same particle number for each value of volume fraction and each particle size were randomly generated. A typical case is illustrated in Fig. 1a. The effective conductivity value for each parameter combination is an average of the effective conductivity values of the three-different representation of the micro-structures for the same values of particle size and volume fraction. Fig. 1b shows how different microstructures with different number of particles (N) with varying particle size (r) are generated for a fixed value of volume fraction. The values of volume fraction are controlled to be within 0.05% of the desired value. The generated images have a very high resolution of 1,000 × 1,000 pixel.

4. Evaluation of Effective Conductivity

The effective electrical conductivity values were

evaluated by the help of numerical simulation of the randomly generated representative microstructures shown in the previous section. Here we only present concise results based on the extensive study carried out over a range of values c.f. Fig. S2. To evaluate the effective properties of the generated images, Eq. (12) was solved using the MUMPS solver in COMSOL [15]. Mesh dependency tests were carried out and a very fine triangular mesh with more than 0.32 million elements was used for all analyses. Transport was assumed to be dominant in horizontal (x-) direction. For each combination of r, h and ε_{AP}, three different instances of the representative microstructure were simulated to obtain three different values of effective electrical conductivities. These estimates were then averaged to obtain the averaged-effective conductivity value (σ^*). For simplicity, the averaged effective conductivity is simply referred to as conductivity in the following sections.

Fig. 2 shows the effect of particle size (r) on conductivity for four different combinations of volume fraction and conductivity ratios. As seen in this figure, for a given volume fraction, when the particle size of the solid phase decreases, leading to a greater number of particles, conductivity increases. Conductivity is directly related to the number of pathways available for the transport of electrons. For a given volume fraction, with smaller particle size, there are a large number of particles in the domain (c.f. Fig. 1b) and as a result the number of pathways increases exponentially. This in turn increases the effective electrical conductivity. In Fig. 1b, particle size of 0.001 (N = 19,000) corresponds to a much larger number of particles available in the domain compared to the microstructure geometry with particle size of 0.04 (N = 50). Table 1 summarizes the results from one combination of h and ε_{AP} to illustrate this. For same values of h and ε_{AP}, decrease in particle size from r = 0.05 to r = 0.0013 leads to more than seven-fold increase in the conductivity. On the other hand, Bruggeman's relationship, shown in Case III for these cases leads to a value of 0.2530 for both values of r which highlights its limitation based on its inability to incorporate the microstructure geometric information. The error bars, shown as black vertical lines in Fig. 1 represent the variation in the values of σ^* as a result of averaging three different values from the three respective random microstructure topologies for a particular case.

Fig. 3 illustrates the variation in the normalized values of σ^* with the change in volume fraction across a range of particle sizes for two different values of h. As expected effective conductivity is enhanced with increasing volume fraction of the solid phase. A similar trend is observed for all other values of h. The variation of σ^*, across a broad range of values of h, as a function of volume fraction for r = 0.011 is shown in Fig. S3 of the supplementary material. This trend is observed for all other values of r considered in the study.

4.1 Comparison with Effective Bounds and Bruggeman's Formula

Effective property bounds of the randomly generated microstructures provide the upper and lower limits of the expected values of a given property. In this section, we compare the results obtained for the calculation of effective electrical conductivity for a range of microstructures based on the proposed mathematical homogenization method, Weiner bounds and Bruggeman's formula. The Weiner bounds provide the limits of the values of effective properties by utilizing the information on volume fraction and individual conductivities [20]. These Weiner bounds for a two-phase microstructure in terms of the conductivity ratios are given as [13]:

$$\sigma^*_L = \sigma_E \left(\varepsilon_{AP}/h + \varepsilon_E\right)^{-1} \quad (14)$$

$$\sigma^*_U = \sigma_E \left(\varepsilon_{AP} \times h + \varepsilon_E\right)^{-1} \quad (15)$$

The comparison between the values for effective conductivity obtained from homogenization method, Weiner bounds and Bruggeman's formula is shown in Fig. 4. Since Weiner bounds and Bruggeman's formula only use the information of volume fraction and individual conductivities, the values based on them are

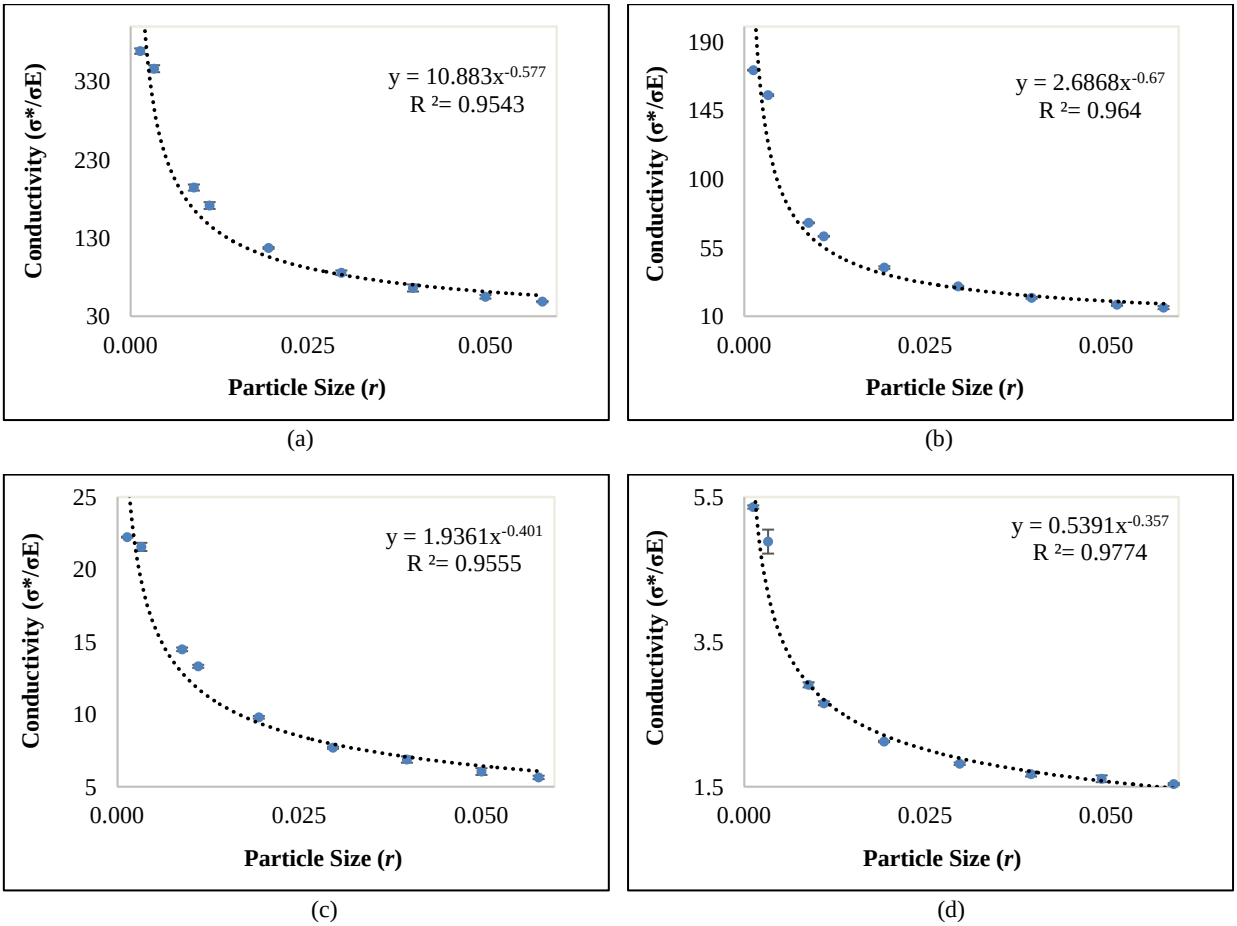

Fig. 2 Variation of effective conductivity values with particle size (*r*) for: (a) *h* = 50, ε_{AP} = 0.1; (b) *h* = 50, ε_{AP} = 0.45; (c) *h* = 1,000, ε_{AP} = 0.2, (d) *h* = 1,000, ε_{AP}=0.4. Conductivity is well correlated by the power law equation for all of these cases.

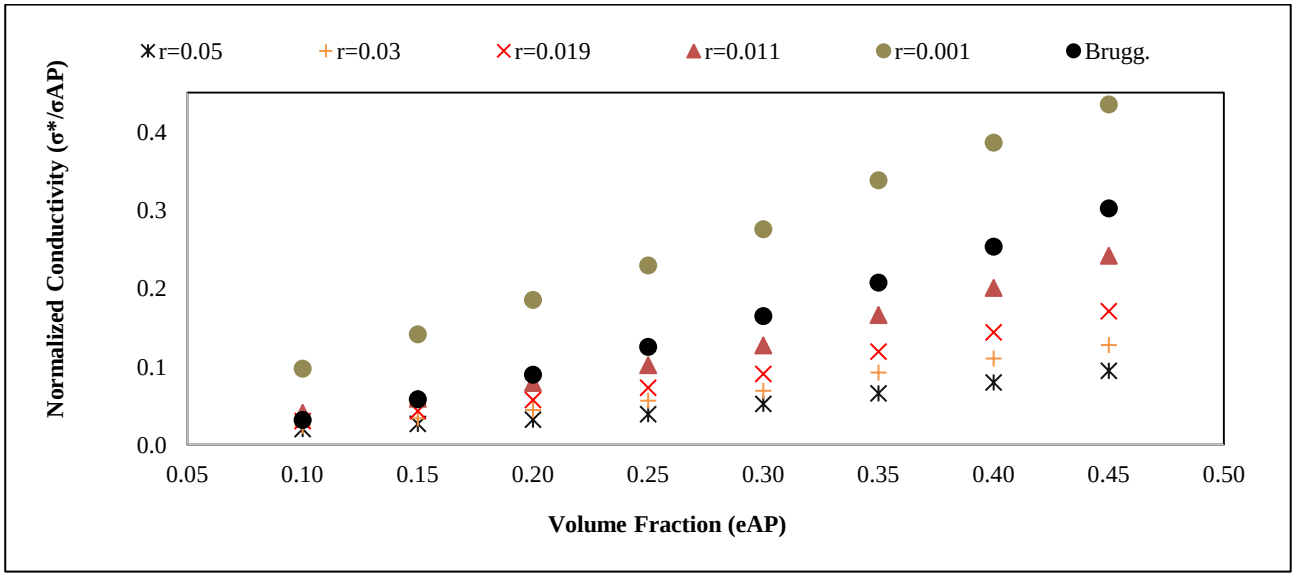

Fig. 3 Variation of normalized effective conductivity with volume fraction for different microstructures with different radii for *h* = 10.

Table 1 Variation in values of σ*.

Case	*h*	ε_{AP}	*r*	σ^*/σ_{AP}
I	10^6	0.45	0.05	0.0481
II	10^6	0.45	0.0013	0.3586
III	10^6	0.45	(0.05, 0.0013)	0.2530

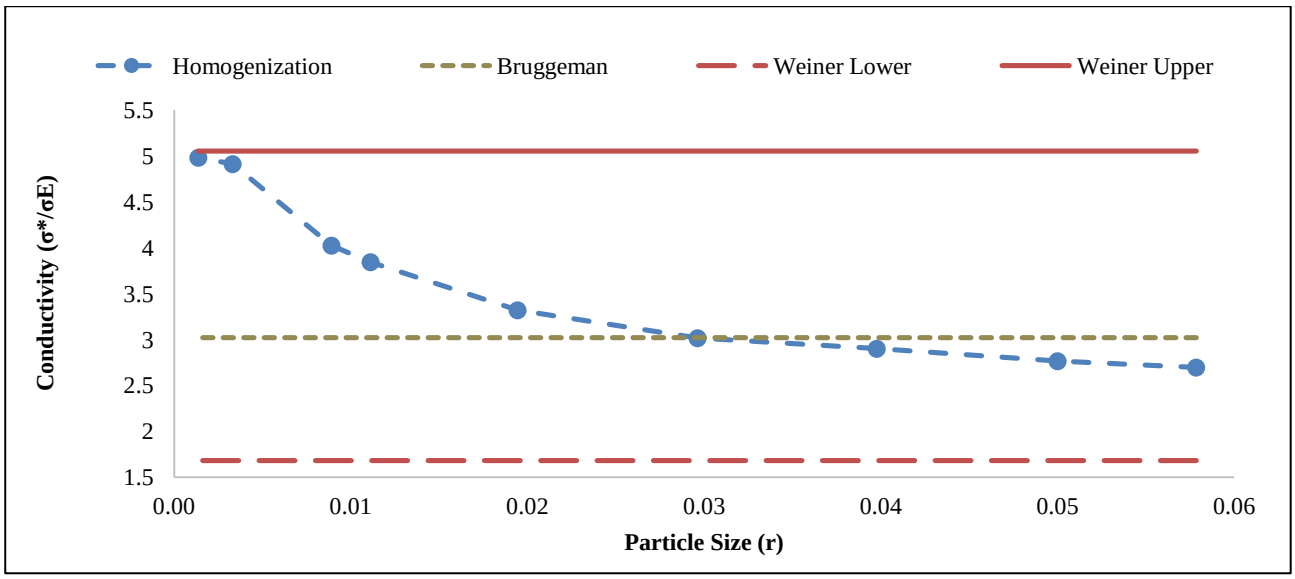

Fig. 4 Comparison of effective conductivity values from the homogenization technique with Bruggeman's formula for microstructures as a function of the particle size for *h* = 10 and ε_{AP} = 0.45.

Table 2 Variation of τ and corresponding values of coefficients *c* and γ for different values of *r*.

r	*c*	γ	τ (ε_{AP} = 0.3)
0.05	5.2394	1.4901	9.4525
0.01	2.3170	1.2824	3.2553
0.001	0.7209	1.0346	0.7516

the same for all particle sizes. However, the homogenization method, used in this study which utilizes the information of microstructural geometry, provides different values for different particle sizes. Put differently, the microstructure varies as the particle size changes and this method is able to take into account. These conductivity values across the spectrum of particle sizes fall within the rigorous Weiner bounds.

4.2 Evaluation of Tortuosity

Tortuosity is a parameter which is used to provide an indication of the difficulty of transport of the species through a microstructure. The relationship between τ and ε_{AP} can be written as:

$$\tau = \varepsilon_{AP}^{-0.5} \quad (16)$$

Thorat et al. [17] provided the following relationship between tortuosity and porosity :

$$\tau = c\,\varepsilon_{AP}^{1-\gamma^s} \quad (17)$$

Most research works in this field use Eq. (16) by setting the value of c = 1 and γ = 1.5 in Eq. (18) [17]. Fig. S4 shows the comparison between tortuosity and volume fraction of the solid conductive phase for different particle sizes. The values of tortuosity based on Bruggeman's formula are the same for different particle sizes for a given value of ε_{AP}. A detailed analysis of the relationship between τ and r is presented for the case of ε_{AP} = 0.3 as shown in Table 2. As the particle size increases from r = 0.001 to r = 0.05, the microstructure topology changes significantly and the value of τ increases by almost thirteen times. For a given volume fraction, there are more active particles

available for electrical conduction when the size of particles is small. However, when the size of the particles increases, the number of active particles distributed throughout the electrode becomes smaller. This leads to a significantly fewer pathway for the transport of electrons leading to a higher value of τ, i.e., a more tortuous path for the electrons to move. Now, using the structure of Eq. (17), we can obtain the values of the constants c and Bruggeman's exponent γ for each value of *r* as summarized in Table 2. These expressions are very different from the one given in Eq. (17). Kehrwald et al. [21] also reported similar differences between their derived expressions and the one described by Bruggeman's relation. Similarly, there is an increase in the possible conductive pathways for the electrons to travel with the increase of volume fraction. Hence, with the increase in the values of ε_{AP}, the values of τ decreases as shown in Fig. S4 of the supplementary material.

4.3 Algebraic Formulation to Evaluate Effective Conductivity

It is evident from the results of the previous sections, the effective conductivity varies with the variation of conductivity ratio, particle size and volume fraction of active particles. The relationships between effective conductivity and these three parameters are found to follow certain trends across a wide spectrum of values of *h*, *r* and ε_{AP}. Based on these trends, we propose an explicit formulation for the effective electrical conductivity as a function of conductivity ratio *h*, particle size *r* and volume fraction of solid phase ε_{AP}:

$$\sigma^* = \mathrm{f}(\mathrm{h}, \mathrm{r}, \varepsilon_{\mathrm{AP}}) \tag{18}$$

Algebraic manipulations of the relationships between σ* and *h*, *r* and ε_{AP} lead to:

$$\sigma^*/\sigma_{\mathrm{E}} = \mathrm{A}_1(\mathrm{h}) \times \mathrm{r}^{\mathrm{B}_1(\mathrm{h})} \times \varepsilon_{\mathrm{AP}}^{\mathrm{A}_2(\mathrm{h})\mathrm{r}^{\mathrm{B}_2(\mathrm{h})}} \tag{19}$$

where A_i and B_i are coefficients that are a function of *h*.

The coefficients A_i and B_i in Eq. (19) are found to change with the variation in the values of conductivity ratio. Fig. S5 of the supplementary material shows that the variation of the coefficients of the formulation (A_1, A_2, B_1 and B_2) across a range of values of *h* for $h > 100$ in log scale is in a perfect agreement with the trend line. Based on this, these coefficients in general form can be written as:

$$A_1 = A_{11}.h^{A_{12}} \tag{20}$$

$$B_1 = B_{11}.h^{B_{12}} \tag{21}$$

$$A_2 = A_{21}.h^{A_{22}} \tag{22}$$

$$B_2 = B_{21}.\ln(h) + B_{22} \tag{23}$$

Similarly, an analysis was carried out for the values of $h \leq 100$, and coefficients in Eqs. (20)-(23) were obtained. The values of the coefficients for the two ranges of *h* are summarized in Table 3. In the next section, a rigorous analysis of the proposed formulation is carried out.

4.4 Analysis of the Proposed Formulation

In this section, we analyze the formulation proposed in Eq. (19) that describes the effective electrical conductivity as a function of particle size, volume fraction and conductivity ratio. For the analysis, 200 different combinations of *r*, *h* and ε_{AP} were considered. Fig. 5 shows a comparison of the effective conductivity values from Eq. (19) and the mathematical homogenization method. An average relative error value of approximately 8% was obtained. Major sources of errors are the errors of estimate accumulated because of the use of multiple trend lines for prediction and the cut-off value for volume fraction (~0.05%) used to save computational time.

To show that Eq. (19) proposed in this study is valid of solid-phase particles of various shapes, three other theoretical shapes of the active particles were considered. Fig. 6a shows the representative microstructures with these three shapes, namely square, triangle and circle. The particle size for these shapes is defined according to the definition provided in the representative microstructure generation section. Effective conductivity values were obtained for a range of values of *h*, *r* and ε_{AP} from mathematical homogenization technique as well as the formulation proposed in Eq. (19).

Table 3 Value of coefficients of the algebraic formula for calculation of effective conductivities.

h	A_{11}	A_{12}	B_{11}	B_{12}	A_{21}	A_{22}	B_{21}	B_{22}
$h \leq 100$	0.7136	0.4076	0.1189	0.3219	0.1676	0.4173	0.0379	0.17198
$h > 100$	0.0503	0.9885	0.4957	0.0014	1.7349	0.0079	0.0013	0.07232

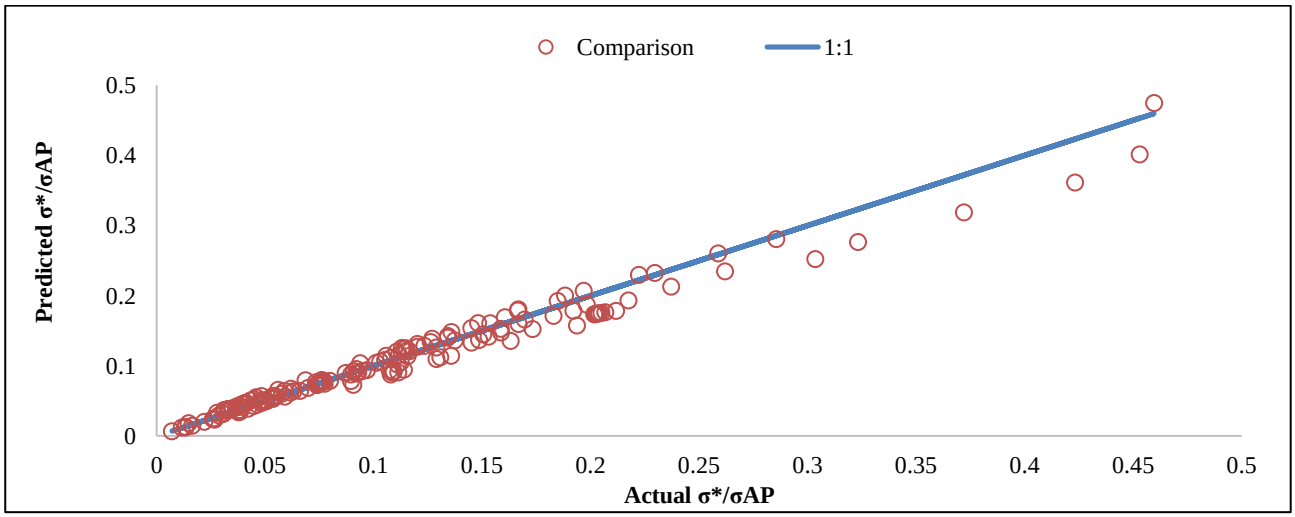

Fig. 5 Comparison of the explicit formulation predicted values of conductivity normalized by conductivity ratio with the actual values from simulation based on homogenization method across a range of values of h, r and ε_{AP}.

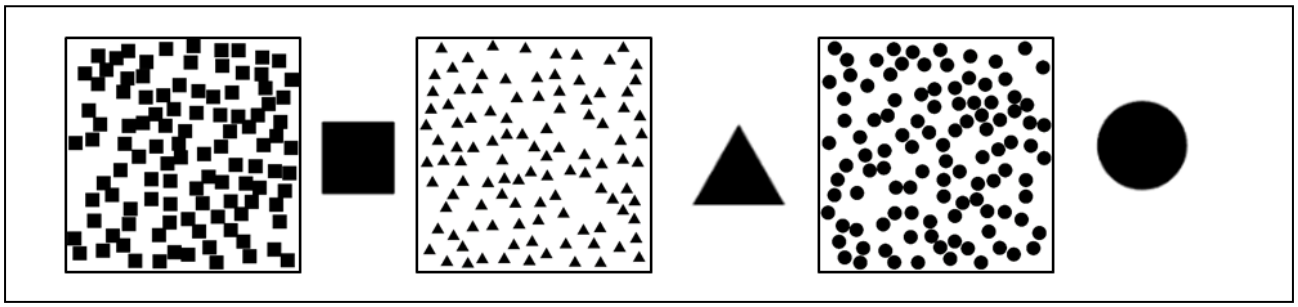

(a)

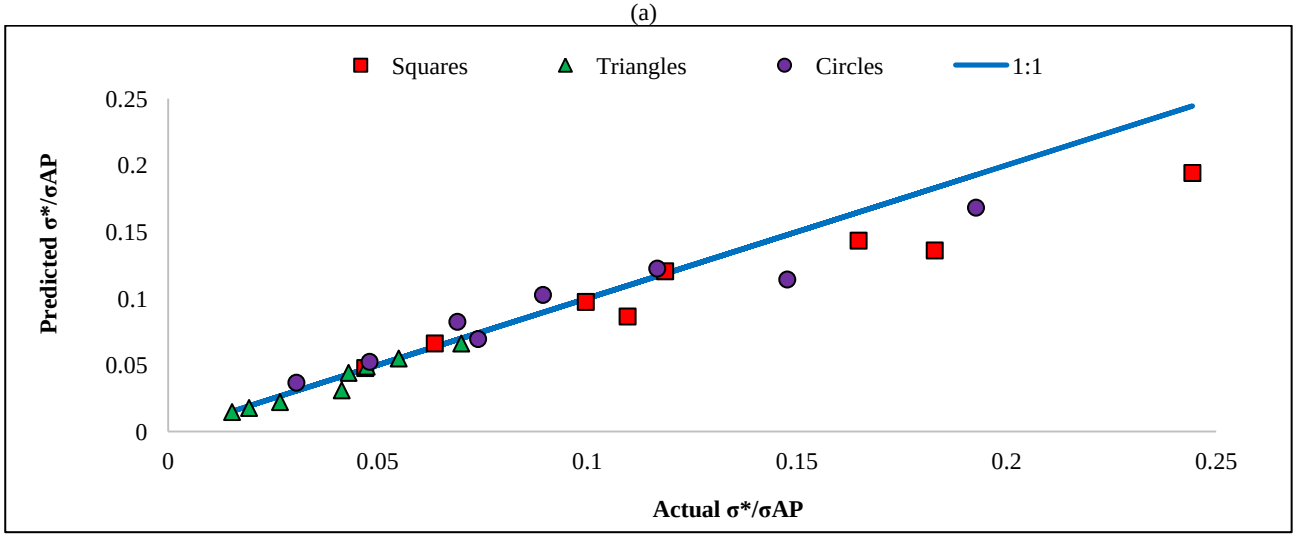

(b)

Fig. 6 (a) Microstructures of square, triangular and circular shapes from left to right with magnified views of shapes for different values of r and ε. (b) Comparison between predicted values of normalized conductivity using proposed formulation with actual values based on homogenization method for different shapes of solid-phase particles.

A comparison of the results from Eq. (19) (predicted values) and the homogenization technique (actual values) is presented in Fig. 6b. Once again, we observe a strong correlation between the actual and predicted values. The average relative errors for the square, triangular and circular shapes are approximately 11%, 8% and 14% respectively.

The proposed formula can be used to evaluate the effective electrical conductivity of the positive electrode of a Li-ion battery consisting of electrolyte and the active materials as discussed. However, the Li-ion batteries in use now also include three phases. Fig. S6 shows typical positive electrode microstructure images as it undergoes changes during a typical charge and discharge cycle. Although this formulation cannot be directly used for the evaluation of effective electrical conductivity because of the presence of the binder phase, it can prove useful for additive-free cathodes as discussed earlier. Hence, it provides an easy way to evaluate the effective electrical conductivity of a cathode consisting of two distinct phases viz. electrolyte and active particles.

5. Application Performance of a Li-ion Cell Model

In this section, we illustrate the application of the proposed formulation by providing the results and analysis of a Li-ion cell model which is based on the study on P2D model developed by Doyle et al. [18]. This model is based on the principles of electrochemistry, transport phenomena and thermodynamics and has been extensively used to study battery models. Taleghani et al. [10] used this model to study the effects of porosity and particle size distribution on the performance of Li-ion battery. Similarly, Prada et al. [22] used this model to provide a simplified model for $LiFePO_4$-graphite Li-on batteries. Here, we study the influence of microstructure on cell discharge characteristics using this P2D model. Mono-modal particle size distribution is considered for the study. This section aims to highlight the importance of accurate prediction of effective properties by considering the microstructure geometry using the effective property values evaluated using the proposed formulation based on the mathematical homogenization method. We also highlight the limitation of Bruggeman's formula on battery performance prediction.

The schematic diagram model of Li-ion battery considered for study is shown in Fig. 7. This model is based on a study carried out by Doyle et al. [18]. Here, we use two distinct phases as described earlier and consider the active particles and electrolyte in both electrodes. $LiPF_6$ salt dissolved in organic solvent 1:2 *v*/*v* mixture of EC: DMC with the polymer matrix, p(VdF-HFP) is the electrolyte used in this study. The negative electrode is composed of carbon-based material whereas the positive electrode consists of $Li_xMn_2O_4$.

Values of different parameters used in this study are summarized in Table 4. Most of the parameters including the properties of electrodes and electrolyte used here are based on the study by Doyle et al. [18]. For all other key parameters used in this electrochemical model, the reader is referred to COMSOL's documentation [15].

In the study, electrical conductivity of electrolyte is assumed to be 10^{-8}. This value leads to a conductivity ratio h of nearly 10^8 and 10^{10} for positive and negative electrodes respectively. This value is generally assumed to be zero in literature. But the homogenization method used in this study does not allow us to consider a value of zero [13]. Here, we only modify effective electrical conductivity using the proposed homogenization-based formulation. The results based on the effective conductivity calculated using homogenization method are then compared to the results obtained based on the correction given by Bruggeman's formula. Effective values of ionic conductivity and diffusivity are based on Bruggeman's formula by default and are unchanged. The MUMPS direct solver is used for all simulations in COMSOL for this study [15].

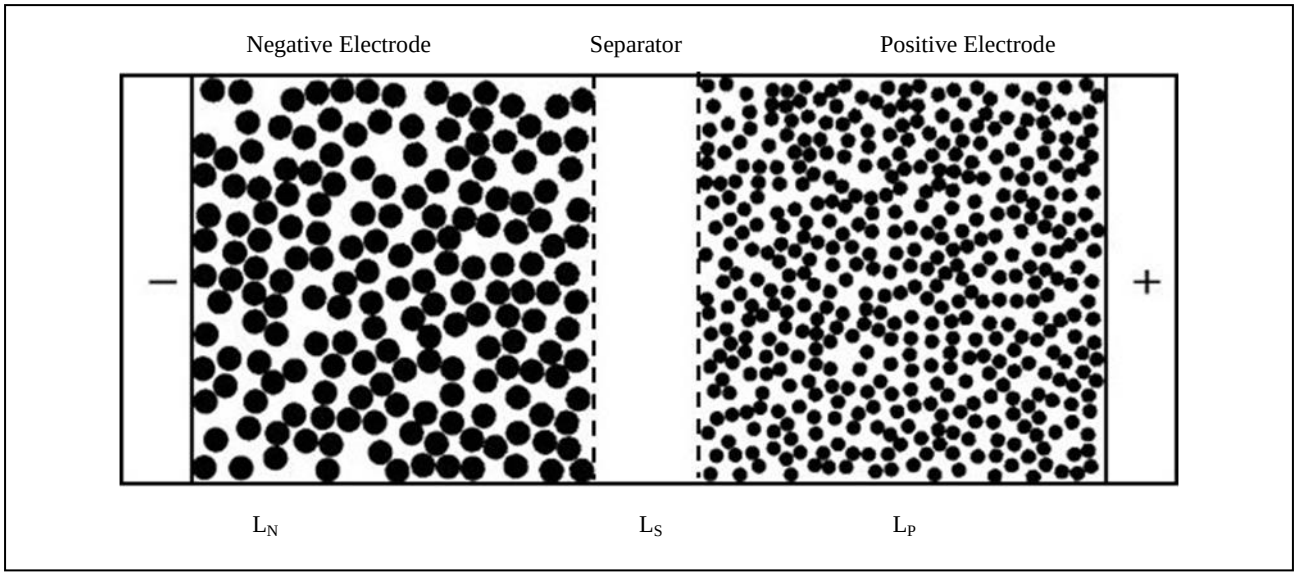

Fig. 7 Schematic diagram of Li-ion cell consisting of positive electrode, separator and negative electrode. The positive and negative porous electrodes both are shown to consist of two phases with the white phase representing electrolyte.
The dark circular inclusions denote the active materials which are carbon and lithium manganese dioxide particles for positive and negative electrodes respectively. The current collectors for the negative and positive electrodes are represented by – and + respectively.

Table 4 Key parameters for the electrodes.

Parameter	Positive electrode	Negative electrode
Active material	$Li_xMn_2O_4$	Li_xC_6
L*	174 μm	100 μm
σ_{AP}	3.8 S/m	100 S/m
r_p	8.5 μm	12.5 μm
ε_{AP}	0.3	0.45
ε_E	0.7	0.55
h	3.8×10^8	10^{10}

*The width of separator is 52 μm.

In Fig. 8a, we show the discharge curves at the discharge rates of 4C and 8C using the effective electrical conductivity values calculated using the Bruggeman's formula and the proposed homogenization-based formulation. In this case, the theoretical 1C-rate current density is 17.5 A/m^2 [18]. The discharge capacity decreases at an increasing rate for a given cell voltage when the discharge rate increases from 4C to 8C. The cell discharge capacity decreases by 65% at a discharge rate of 8C as compared to that at 1C based on Bruggeman's estimate at 3V. On the other hand, this change in discharge capacity is 69% when we use the homogenization-based formulation.

At 8C, the 3V discharge capacity of the cell is almost 14% lower based on homogenization approach as compared to Bruggeman's formula. And this difference at different cell voltage values increases with increasing discharge rate as shown in Fig. 5. It is important to note that this deviation could be even larger if we were to use the homogenization approach for the evaluation of effective diffusivity and electrolyte conductivities. This further highlights the need for the use of microstructure geometry information while evaluating the effective properties.

In Fig. 8c, we show the discharge characteristics with the change in the active particle sizes at 1C. Table 5 includes the values of the Bruggeman's exponent (γ)

that should be used based on the homogenization formulation instead of the idealized value of $\gamma = 1.5$ for three different cases. For case A, the value of γ is 3.842. This value is more than twice the value proposed by Bruggeman's formula. This is supported by the results from the previous studies [18].

Decrease in particle size for the same values of volume fraction leads to greater number of pathways for electronic conduction because of the presence of more active particles. Consequently, better discharge characteristics are observed. As the active particle sizes for both electrodes are decreased by 25% (cases A and C) based on the homogenization-based formulation, the value of discharge capacity for a cell voltage of 3 V at the discharge rate of 1C increases by almost 80%. Similarly, the difference between the discharge characteristic curves based on homogenization and Bruggeman's formula keeps on increasing with increasing discharge rates as shown in Figs. 8a and 8b.

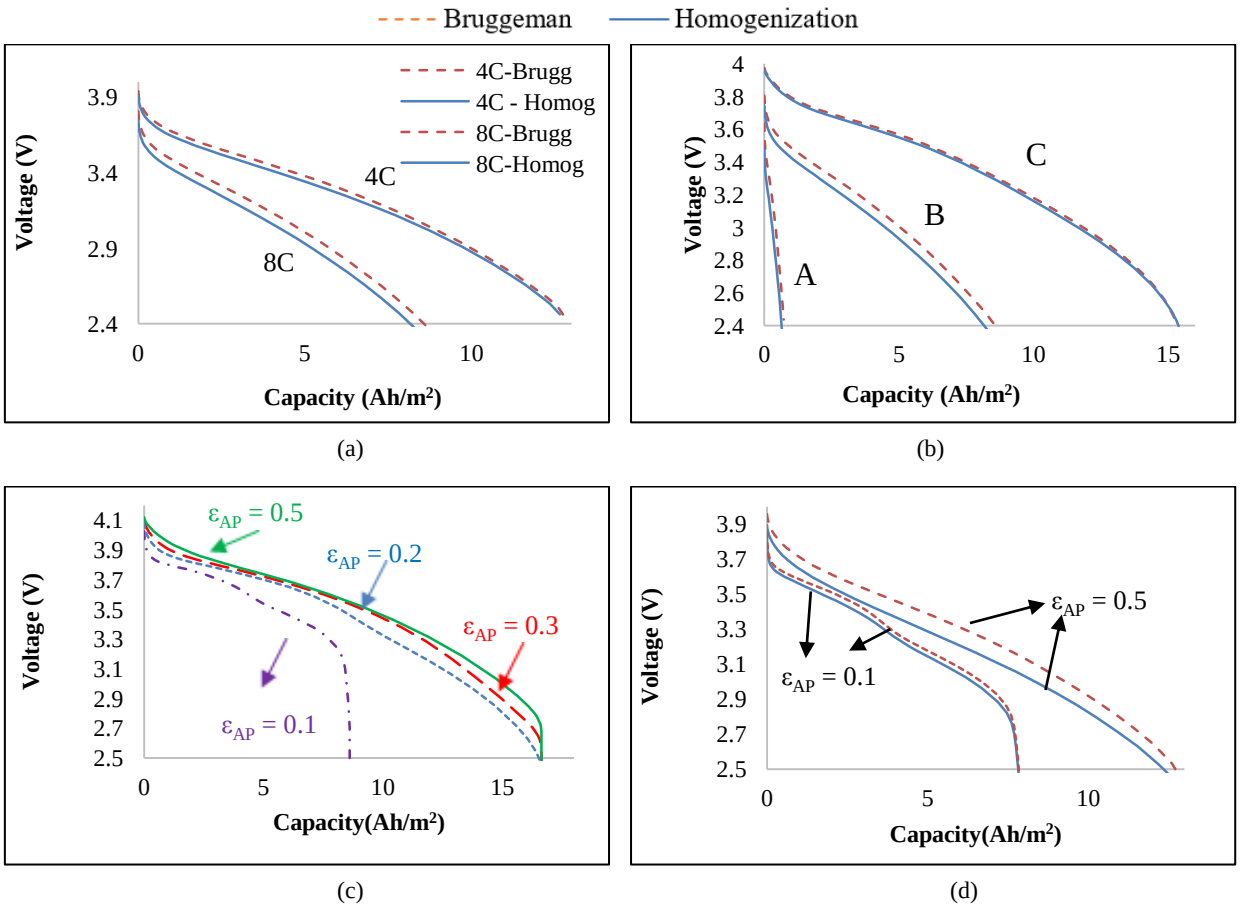

Fig. 8 Results for the Li-ion cell. (a) Discharge rate comparison at discharge rates of 4C and 8C. (b) Discharge curves for cases A, B and C. (c) Discharge rates for different values of volume fraction at 1C. (d) Discharge rate comparison for different values of volume fraction at 1C.

Table 5 Cases with variation of active particle sizes and corresponding values of σ* and γ.

Case	Positive electrode			Negative electrode		
	r_p (μm)	σ* (S/m)	γ	r_n (μm)	σ* (S/m)	γ
A	42.5	0.037	3.842	62.5	1.008	5.758
B	8.5	0.115	2.903	12.5	2.921	4.425
C	1.7	0.341	2.001	2.5	8.162	3.138

As a result of the increase in volume fraction means, greater amount of active materials become available for conduction. This leads to better discharge characteristics. In Fig. 8c, we show the discharge curves by varying only the volume fraction and corresponding effective electrode conductivity for the positive electrode only using the proposed formulation at a discharge rate of 1C. With the increase in volume fraction of the active particles in the positive electrode, a considerable improvement in the discharge characteristics can be observed. At 3 V cell voltage, the capacity increases by 76% as this volume fraction increases from 0.1 to 0.5. In Fig. 8d, we show the discharge characteristics for different values of volume fractions using both the described methods. It can be observed that for both values of volume fraction, values based on Bruggeman's formula overpredict the voltage at a given discharge capacity.

6. Summary and Conclusions

In this study, the focus has been on two-phase electrodes without any additives to enhance conductivity. We show that by carefully engineering the microstructures, we can enhance the effective properties. To this end, we have carried out an extensive analysis of the effective electrical conductivity of randomly generated microstructures idealized for Li-ion battery electrodes using mathematical homogenization based approach. The Bruggeman's formula cannot factor in the change in microstructure geometry. Therefore, it is only able to predict a constant value of effective conductivity for all particle sizes. On the other hand, homogenization based technique considers the microstructure geometry and gives different values based on microstructure geometry.

From the results of mathematical homogenization, to provide a simple method for the evaluation of effective electrical conductivity of an electrode of a Li-ion battery based on the conducting solid phase and non-conducting electrolyte phase, we have proposed an explicit formula relating effective conductivity with conductivity ratio of phases, particle size and volume fraction of active phase. We have also carried out an analysis of the proposed formulation showing a very good agreement with the actual values based on homogenization method for a mono-modal particle size distribution.

To highlight the applicability of the proposed formulation, the discharge characteristics were studied for a Li-ion battery based on the P2D model. We present the differences in the discharge curves when the microstructural effect is considered with the homogenization method and when it is not using the Bruggeman's formula. It was observed that the variation between results of discharge characteristics based on these two approaches is more significant at higher discharge rates and for higher volume fraction of active particles.

A possible extension to this work could be to include multi-modal particle size distribution to provide a more accurate representation of the effective values. Similarly, in order to overcome the limitation with the confinement of transport of properties in a single plane, results for the evaluation of the effective electrical conductivity based on the depth of the electrodes can be studied in the future. Finally, inclusion of other effective properties including diffusivity and ionic conductivity would be able to provide a more accurate description of the discharge characteristics of the battery model.

Acknowledgments

Both authors are grateful to NSERC for funding this work via the Discovery grant program.

References

[1] U.S. Energy Information Administration,2016. "International Energy Outlook 2016".

[2] World Energy Council. 2016. "World Energy Scenarios 2016".

[3] Lu, J., Chen, Z., Ma, Z., Pan, F., Curtiss, L. A., and Amine, K. 2016. "The Role of Nanotechnology in the

Development of Battery Materials for Electric Vehicles." *Nat. Nanotechnol*. 11 (12): 1031-8.

[4] Yu, D. Y. W., Yanagida, K., Kato, Y., and Nakamura, H. 2009. "Electrochemical Activities in Li_2MnO_3." *J. Electrochem. Soc.*. 156 (6): A417-24.

[5] Silberberg, M. S., and Amateis, P. 1996. *Chemistry: The Molecular Nature of Matter and Change.* McGraw Hill.

[6] Ha, D. H., Ly, T., Caron, J. M., Zhang, H., Fritz, K. E., and Robinson, R. D. 2015. "A General Method for High-Performance Li-Ion Battery Electrodes from Colloidal Nanoparticles without the Introduction of Binders or Conductive-Carbon Additives: The Cases of MnS, $Cu_{2-x}S$, and Ge." *ACS Appl. Mater. Interfaces* 7 (45): 25053-60.

[7] Liu, C., Neale, Z. G., and Cao, G. 2016. "Understanding Electrochemical Potentials of Cathode Materials in Rechargeable Batteries." *Biochem. Pharmacol.* 19 (2): 109-23.

[8] Fergus, J. W. 2010."Recent Developments in Cathode Materials for Lithium Ion Batteries." *J. Power Sources* 195 (4): 939-54.

[9] Chung, D.-W., Ebner, M., Ely, D. R., Wood, V., and Edwin Garcá, R. 2013. "Validity of the Bruggeman Relation for Porous Electrodes." *Model. Simul. Mater. Sci. Eng*. 21 (7): 74009.

[10] Taleghani, S. T., Marcos, B., Zaghib, K., and Lantagne, G. 2017. "A Study on the Effect of Porosity and Particles Size Distribution on Li-Ion Battery Performance." *J. Electrochem. Soc.* 164 (11): E3179-89.

[11] García, R. E., Chiang, Y.-M., Craig Carter, W., Limthongkul, P., and Bishop, C. M. 2005. "Microstructural Modeling and Design of Rechargeable Lithium-Ion Batteries." *J. Electrochem. Soc.* 152 (1): A255.

[12] Ramadesigan, V., Northrop, P. W. C., De, S., Santhanagopalan, S., Braatz, R. D., and Subramanian, V. R. 2012. "Modeling and Simulation of Lithium-Ion Batteries from a Systems Engineering Perspective." *J. Electrochem. Soc.* 159 (3): R31-45.

[13] Gully, A., Liu, H., Srinivasan, S., Sethurajan A. K., Schougaard, S., and Protas, B. 2014. "Effective Transport Properties of Porous Electrochemical Materials—A Homogenization Approach." *J. Electrochem. Soc.* 161 (8): E3066-77.

[14] Bruggeman, D. A. G. 1935. "Berechnung Verschiedener Physikalischer Konstanten von heterogenen Substanzen. I. Dielektrizitätskonstanten und Leitfähigkeiten der Mischkörper aus isotropen Substanzen." *Ann. Phys.* 416 (7): 636-64.

[15] COMSOL Inc. "COMSOL Multiphysics Modeling Software."

[16] Vadakkepatt, A., Trembacki, B., Mathur, S. R., and Murthy, J. Y. 2016. "Bruggeman's Exponents for Effective Thermal Conductivity of Lithium-Ion Battery Electrodes." *J. Electrochem. Soc.* 163 (2): A119-30.

[17] ThoratI, V., Stephenson, D. E., Zacharias, N. A., Zaghib, K., Harb, J. N., and Wheeler, D. R. 2009. "Quantifying Tortuosity in Porous Li-Ion Battery Materials." *J. Power Sources* 188 (2): 592-600.

[18] Doyle, M., Newman, J., Gozdz, A. S., Schmutz, C. N., and Tarascon, J. 1996. "Comparison of Modeling Predictions with Experimental Data from Plastic Lithium Ion Cells." *J. Electrochem. Soc.* 143 (6): 1890.

[19] The MathWorks Inc. "Image Processing Toolbox—MATLAB."

[20] Golden, K. 1986. "Bounds on the Complex Permittivity of a Multicomponent Material." *J. Mech. Phys. Solids* 34 (4): 333-58.

[21] Kehrwald, D., Shearing, P., and Brandon, N. 2012. "Local Tortuosity Inhomogeneities in a Lithium Battery Composite Electrode." *Electrochem* 158 (12): A1393-9.

[22] Prada, E., Di Domenico, D., Creff, Y., Bernard, J., Sauvant-Moynot, V., and Huet, F. 2012. "Simplified Electrochemical and Thermal Model of $LiFePO_4$-Graphite Li-Ion Batteries for Fast Charge Applications." *J. Electrochem. Soc.* 159 (9): A1508-19.

Supplementary Material

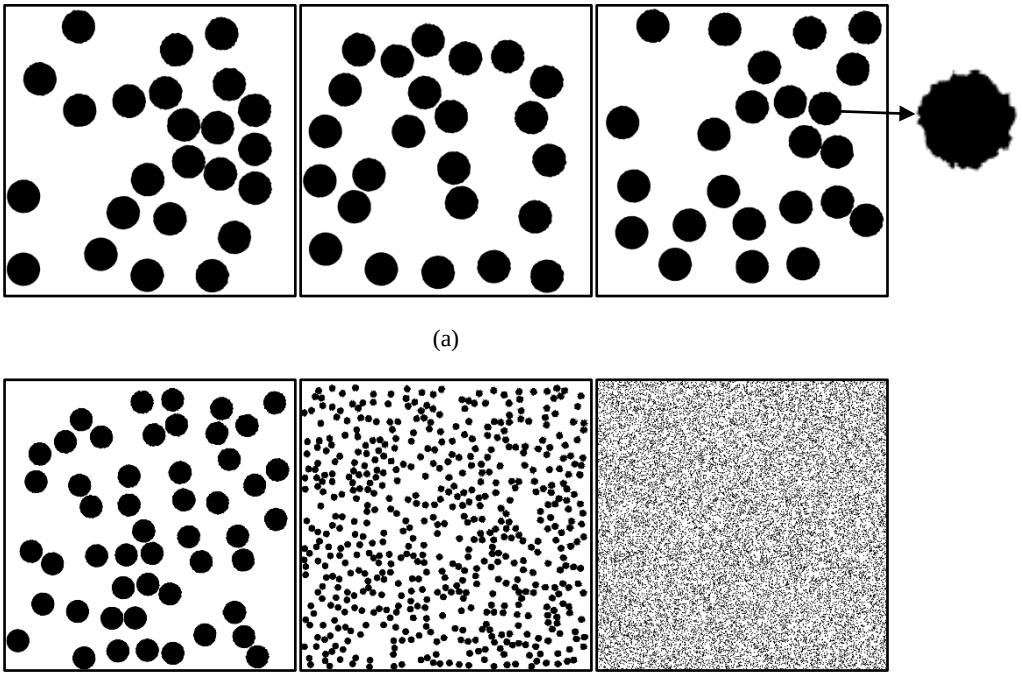

(a)

(b)

Fig. S1 Microstructures generated for study. (a) Three iterations for the same radius of 0.06 and volume fraction of 0.25 with magnified view of one solid phase particle with irregular edges. (b) Different microstructures for same volume fraction but different radii of approximately 0.04 (*N* = 50), 0.011 (*N* = 553) and 0.001 (*N* = 19,894) respectively from left to right.

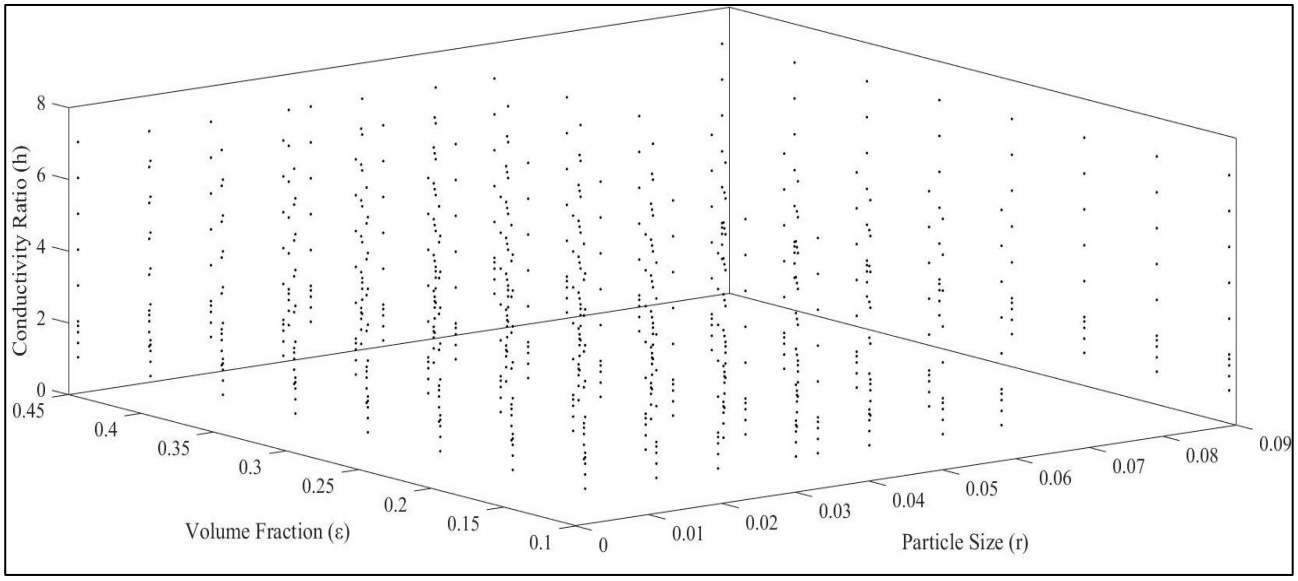

Fig. S2 Range of values used for study. The values of conductivity ratio (*h*) are represented in Log_{10} scale. A total of 720 distinct combinations of *h*, *r* and ε were used for the study and 3 randomly generated microstructures were used for each combination to evaluate the averaged effective conductivity.

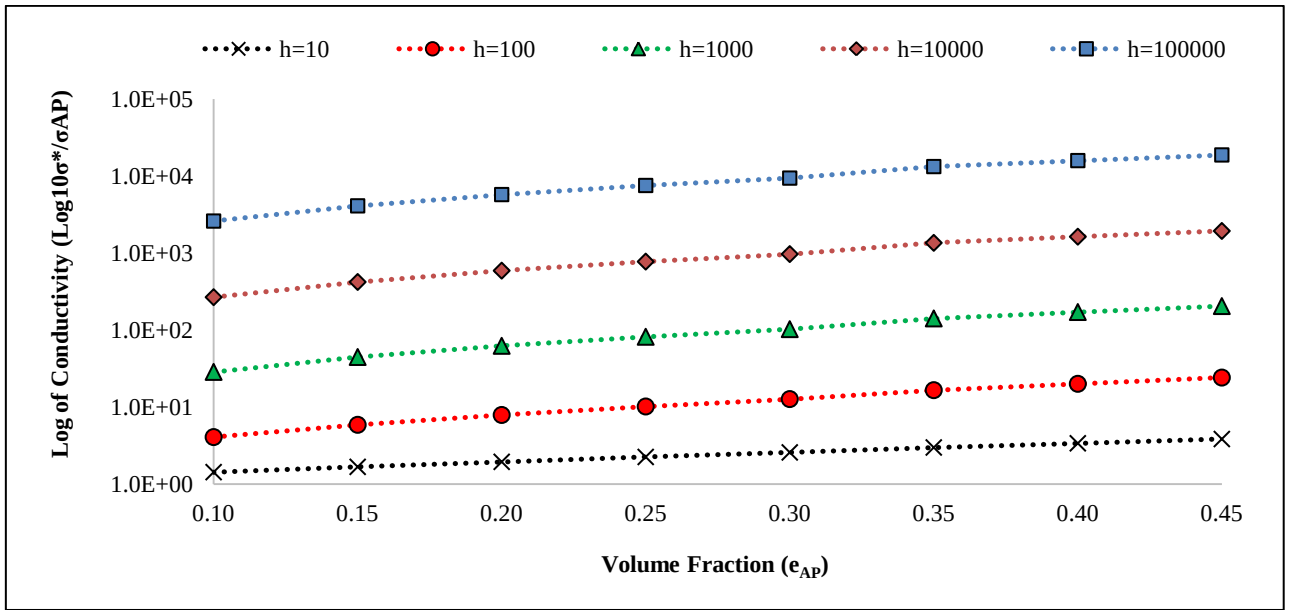

Fig. S3 Effective conductivity as a function of volume fraction for different values of conductivity ratios (r = 0.011).

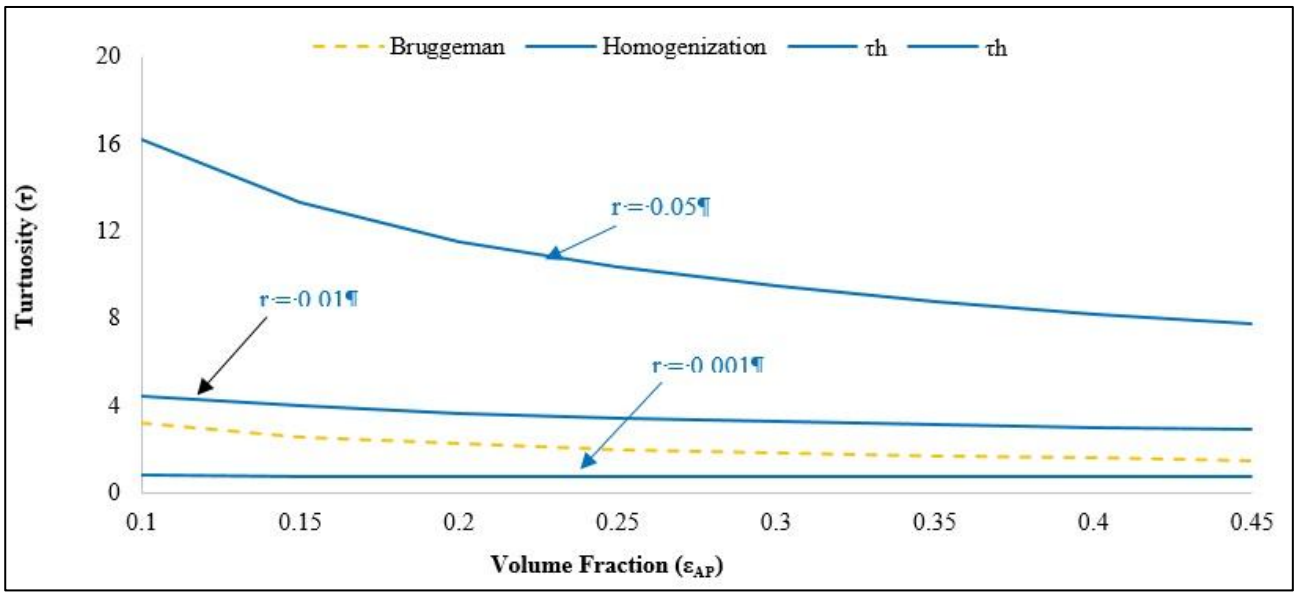

Fig. S4 Comparison of tortuosity vs. volume fraction for different radii based on the mathematical homogenization method with Bruggeman's formula for different microstructures with different radii for $h = 10^7$.

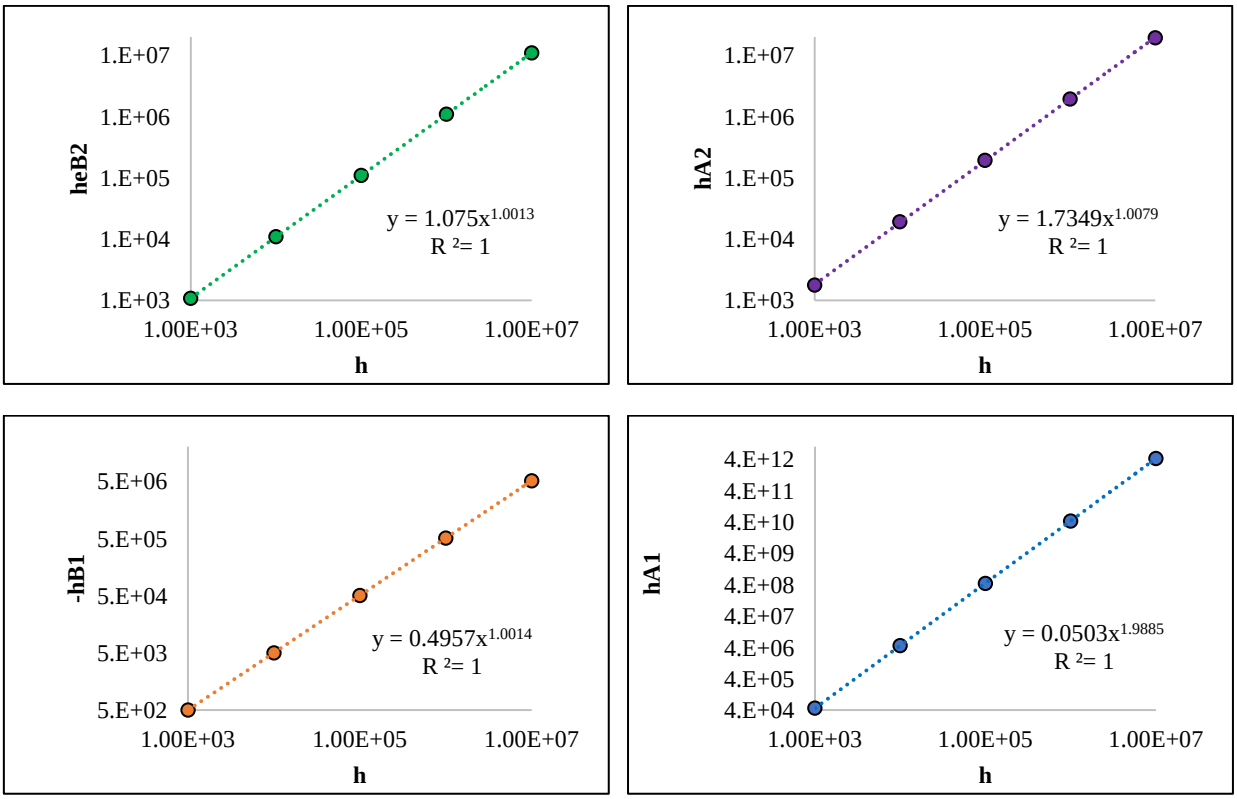

Fig. S5 Variation of the coefficients of formulation A_1, A_2, B_1 and B_2 across a range of values of *h* for *h* > 100. For clarity of representation, both axes are presented in logarithmic scale and the y-axis values are scaled by *h*.

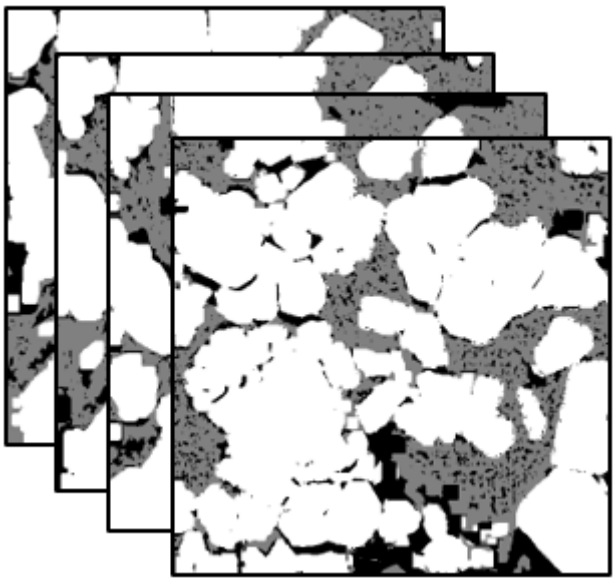

Fig. S6 Processed representative images of a Li-ion positive electrode taken at various stages of the cycling process.